Article

Discovery Medicine 2025; 37(202): 2514–2529
https://doi.org/10.24976/Discov.Med.202537202.211

Functional Integration of Genetically Engineered Porcine Heart–Kidney Grafts in Rhesus Macaques: A Preclinical Model of Multiorgan Xenotransplantation

Licheng Yan[1,†], Zhi Dou[1,†], Chi Zhang[2], Jinfeng Wu[2], Liefu Ye[2], Jun Li[3], Lihua Lei[4], Fuli Wen[5], Haifeng Chen[6], Gang Chen[7], Hua Cao[1,*], Xijie Wu[1,*]

[1]Department of Cardiovascular Surgery, Provincial Hospital Affiliated to Fuzhou University, 350001 Fuzhou, Fujian, China
[2]Department of Urology, Provincial Hospital Affiliated to Fuzhou University, 350001 Fuzhou, Fujian, China
[3]Department of Critical Care Medicine III, Provincial Hospital Affiliated to Fuzhou University, 350001 Fuzhou, Fujian, China
[4]Department of Cardiovascular Anesthesiology, Provincial Hospital Affiliated to Fuzhou University, 350001 Fuzhou, Fujian, China
[5]Animal Experimental Center, Provincial Hospital Affiliated to Fuzhou University, 350001 Fuzhou, Fujian, China
[6]Department of Cardiology, Provincial Hospital Affiliated to Fuzhou University, 350001 Fuzhou, Fujian, China
[7]Department of Endocrinology, Provincial Hospital Affiliated to Fuzhou University, 350001 Fuzhou, Fujian, China
*Correspondence: caohua69@fjmu.edu.cn (Hua Cao); wxjusa@163.com (Xijie Wu)
[†]These authors contributed equally.
Submitted: 1 September 2025 Revised: 18 September 2025 Accepted: 14 October 2025 Published: 20 November 2025

Background: End-stage heart and kidney failure is constrained by donor organ scarcity. This study aimed to establish a standardized protocol for combined heart–kidney xenotransplantation using multi-gene–edited porcine grafts in a non-human primate (NHP) model and to evaluate their short-term functional outcomes, providing a basis for future clinical translation.
Methods: Genetically modified Bama miniature pigs carrying five gene edits (*GTKO*/*SdaKO*/*CD46*/*CD55*/*TBM*) were used as organ donors, and healthy male rhesus macaques served as recipients. Donor hearts and kidneys were harvested using a standardized protocol and preserved via cold perfusion. Cardiac transplantation was performed using an intra-abdominal heterotopic approach, with end-to-side anastomosis between the donor ascending aorta and the recipient abdominal aorta, as well as between the donor pulmonary artery and the recipient inferior vena cava. Renal transplantation involved orthotopic end-to-end anastomosis of the donor renal artery and vein to the recipient's left renal vasculature. A combined immunosuppressive regimen was administered perioperatively, alongside anticoagulation, anti-infective prophylaxis, and supportive care. Recipient vital signs and cardiorenal function were continuously monitored throughout the perioperative period. Experimental endpoints were defined as cessation of renal graft perfusion or irreversible cardiac graft failure.
Results: The recipient survived 7 days and 4 hours post-transplant with stable vital signs. Both grafts demonstrated good intraoperative perfusion. The heart graft resumed beating immediately upon reperfusion, with left ventricular ejection fraction peaking at 35% on postoperative day (POD) 5 before declining. Echocardiography revealed myocardial hypertrophy and reduced contractility, but no complete cardiac failure. The kidney graft showed perfusion by POD 1, and urine output by POD 5 confirmed initial function. However, increased vascular resistance and reversed flow between POD 6 and POD 7 indicated acute graft failure. Laboratory assessments showed persistent anemia, lymphopenia, and intermittent prolongation of activated partial thromboplastin time (APTT). At necropsy, the heart graft retained structural integrity and partial function, whereas the kidney graft exhibited hemorrhagic infarction. Notably, vascular anastomoses remained intact throughout the study. Additionally, the heart graft maintained its function despite renal rejection, suggesting greater resilience to immune injury.
Conclusion: This combined xenotransplantation model demonstrated short-term graft survival, with the cardiac graft showing greater resistance to rejection than the renal graft. It offers a platform for optimizing clinically viable strategies for long-term functional xenotransplantation.

Keywords: xenotransplantation; multi-gene editing; combined heart-kidney transplantation; immune rejection dynamics; non-human primate model

Introduction

The global rise in end-stage organ failure has intensified the critical shortage of donor organs in transplantation medicine [1,2]. Despite steady progress in utilizing living and brain-dead donors, the supply still remains insufficient for the growing clinical demand. In this context, xenotransplantation, particularly using pigs as donors for non-human primates (NHPs) or humans, has become a promising alternative to human allografts, owing to the regenerative potential and scalable availability of porcine donors [3,4]. Pigs are considered optimal donor animals due to their physiological compatibility with humans, suitable organ size, and high reproductive capacity, leading to their widespread use in preclinical xenotransplantation research models [5,6].

In recent years, the advent of multi-gene–engineered pigs has significantly improved immunological compatibility and coagulation control, thereby extending the survival of porcine heart and kidney grafts in NHPs [7,8]. These innovations have led to unprecedented improvements in xenograft survival and function. For example, Singh *et al*. [9] reported a survival period of up to 225 days for porcine heart xenografts in NHPs, while subsequent studies have reported over 400 days of stable function with porcine renal grafts [10], demonstrating considerable breakthroughs in both technical execution and immunomodulatory strategies.

To date, most preclinical xenotransplantation studies have focused on single-organ models, predominantly involving porcine heart or kidney transplantation into NHPs. Heart xenotransplantation studies have reported several months of graft survival under co-stimulation blockade and multi-gene-edited donors [9,11], while kidney xenografts have demonstrated comparably durable function [12]. However, the development of multi-organ transplantation models is increasingly crucial, particularly for clinical contexts involving multi-organ failure or sequential transplant planning. Despite their potential relevance, combined organ xenotransplantation models remain underexplored. Critical concerns, including inter-organ interactions, immunologic challenges, and perioperative management such as anesthesia and hemodynamic support, require further investigation in complex surgical scenarios [13].

Given the prior advances in single-organ xenotransplantation, this study is the first to establish a combined heart–kidney xenotransplantation model, employing five-gene–modified Bama miniature pigs as donors and rhesus macaques as recipients. The model aims to investigate the functional integration and survival of two transplanted organs within the same recipient, thereby providing experimental evidence and technical insights to support future clinical applications of multi-organ xenotransplantation. Furthermore, it gives a comprehensive framework for investigating the physiological and immunological complexities inherent to multi-organ grafts.

Materials and Methods

Experimental Animals

The donor was a five-gene-edited Bama miniature pig (*GTKO*/*SdaKO*/*CD46*/*CD55*/*TBM*) weighing 7.9 kg, obtained from Zhongke Aoge Biotechnology Co., Ltd. (Sichuan, China), with production license SCXK (Chuan) 2020-0033 and animal quality certificate No. 511214800000097. The recipient was a healthy male rhesus macaque weighing 9.4 kg, sourced from Hengshu Biotechnology Co., Ltd. (Sichuan, China), under production license SCXK (Chuan) 2023-0021 and animal quarantine certificate No.51001134187. One donor–recipient pair was used for the current study.

All animals were housed in a temperature-controlled facility (22–25 °C) with a relative humidity of 50–60%, and a 12-hour light/dark cycle. Experimental procedures involving animals were conducted at Haifeng Biotechnology Co., Ltd. (Chengdu, China), under facility license SYXK (Chuan) 2023-0271, and were approved by the Institutional Animal Care and Use Committee (approval number: IAC-202503[O-01]).

Donor Organ Harvest and Preservation

Donor heart and kidney grafts were harvested using a standardized protocol. The organs were preserved via cold perfusion through the ascending aorta for the heart and abdominal aorta for the kidney. Donor pigs were fasted for 12 hours preoperatively with free access to water. Anesthesia was induced with intramuscular ketamine (10 mg/kg) and atropine (0.05 mg/kg), followed by intravenous catheterization, continuous lidocaine infusion (2 mg/kg/hour), and maintenance with 5% isoflurane in oxygen (2.0 L/minute flow).

Heart procurement was performed as follows: After standard sterile draping and a midline sternotomy, the heart was exposed using a retractor. A partial thymectomy was performed, and the pericardium was opened and suspended. A 4-0 Prolene purse-string suture was placed at the aortic root, and a cold perfusion cannula was secured using a Rummel tourniquet. After systemic heparinization (300 U/kg), the ascending aorta was cross-clamped. The inferior vena cava was incised to drain the right atrium, and the left inferior pulmonary vein was opened to drain the left atrium. Furthermore, to induce rapid hypothermia, the mediastinum was packed with sterile crushed ice. A single dose of 4 °C histidine–tryptophan–ketoglutarate (HTK) solution (30 mL/kg; Custodiol, F. Köhler, Germany) was perfused via the ascending aorta at a 20–30 mmHg for approximately 8 minutes. After perfusion, the heart was then excised intact, with the aorta and pulmonary artery trimmed, and orifices of the superior vena cava, inferior vena cava, and pulmonary vein closed by continuous suturing using 6-0 Prolene. The harvested heart was placed in a sterile plastic bag containing 300 mL of 4 °C HTK solution and stored on crushed ice until transplantation.

Kidney procurement was conducted using a dual cannulation approach, with a Fr10 silicone catheter inserted into the abdominal aorta and an infusion tube placed in the superior mesenteric vein. Cold perfusion was performed simultaneously using 1000 mL of renal preservation solution and 1000 mL of UW solution, delivered via a gravity-fed system positioned at a height of 150 cm. After rapid cooling, the liver-kidney organ cluster was excised. The left kidney was then isolated, and the renal artery, vein, and ureter were carefully trimmed for transplantation. After organ retrieval, euthanasia was performed by intravenous injection of sodium pentobarbital (120 mg/kg, P3761, Sigma-Aldrich, St. Louis, MO, USA) via the auricular vein, with confirmation of death by cessation of respiration and cardiac activity.

Preparation of Recipient Animals

Recipient cynomolgus monkeys were fasted for 12 hours before surgery. Sedation was achieved with an intramuscular injection of Stresnil (56 mg), after which the animals were transferred to the operating room. Standard monitoring was initiated upon arrival, including electrocardiography (ECG), peripheral oxygen saturation (SpO_2), non-invasive blood pressure, and rectal temperature. After hair removal and sterile preparation, two peripheral venous access lines were established using 18–22G intravenous catheters inserted on both limbs and secured with sutures and elastic bands.

Oxygen was administered via face mask in conjunction with inhalational isoflurane (1.5–2%). Additional anesthesia was provided with intravenous propofol (0.5–2 mg/kg) and intramuscular atropine (0.02 mg/kg). Endotracheal intubation was performed using a 3.5# single-lumen endotracheal tube, and placement was confirmed by auscultation or fiberoptic bronchoscopy. The tube was secured to the lower jaw with cotton ties to prevent displacement and connected to a mechanical ventilator. Ventilator parameters were adjusted to a tidal volume (VT) of 8–10 mL/kg and a respiratory rate of 20–30 breaths/minute.

Anesthesia was maintained with inhalational isoflurane (1–2%), while analgesia was provided with intravenous meloxicam (0.1–0.2 mg/kg). Invasive arterial pressure monitoring was established via femoral artery cannulation. Central venous access was established based on surgical requirements, using either a 20G single-lumen central venous catheter or a 4F/5F vascular sheath.

Hemodynamic stability was maintained by continuous lidocaine infusion (1–2 mg/kg) and titrated vasopressors (epinephrine or norepinephrine), guided by real-time blood pressure and heart rate monitoring. Fluid replacement was administered using crystalloids, colloids, and packed red blood cells, based on intraoperative losses and body weight.

Systemic anticoagulation was initiated before skin and peritoneal incision. Intravenous heparin (200–300 IU/kg) was administered according to body weight. Intraoperative with activated clotting time (ACT) monitored intraoperatively. A target ACT of 234 seconds was maintained (baseline ACT: 99 seconds), and heparin dosage was dynamically adjusted, with additional doses given as needed to ensure adequate anticoagulation and reduce the risk of thrombosis.

Organ Transplantation

Cardiac Transplantation

A midline abdominal incision was made extending from the xiphoid process to the pubic symphysis, incising both the skin and peritoneum. After retracting the abdominal wall and displacing the intestines laterally to the left, the retroperitoneal space was exposed. The inferior vena cava (IVC) and abdominal aorta were fully mobilized down to the iliac bifurcation, with lumbar arteries and collateral vessels ligated and divided. Following intravenous administration of heparin (300 U/kg), the abdominal aorta was clamped below the renal arteries (liven cardiovascular clamp CSO1660, August Reuchlen GmbH, Tuttlingen, Germany), and the distal end was clamped above the iliac bifurcation (liven cardiovascular clamp CSO1245, August Reuchlen GmbH, Tuttlingen, Germany). An incision was created on the lateral wall of the abdominal aorta and adjusted to match the donor vessel diameter. The donor ascending aorta was then anastomosed to the recipient's abdominal aorta in an end-to-side fashion using 6-0 Prolene sutures, with the final knot left untied at this stage.

The IVC was partially clamped below the renal veins using a side-biting vascular clamp (liven cardiovascular clamp CSO1612, August Reuchlen GmbH, Tuttlingen, Germany). A longitudinal incision was then made in the anterior wall of the IVC and adjusted to the appropriate size, followed by an end-to-side anastomosis of the donor pulmonary artery to the recipient IVC using 6-0 Prolene sutures, with the final knot left untied initially. Once both anastomoses were prepared, a 20G cannula was inserted into the arterial anastomosis, and 20 mL of 4 °C HTK solution was flushed through to expel residual air from the anastomotic lumens. The arterial and venous anastomoses were then secured, and blood flow was sequentially restored first to the veins and then to the arteries.

Following reperfusion of the donor heart, ventricular fibrillation frequently occurred but was successfully reversed with a 5 J electrical defibrillation, restoring spontaneous cardiac rhythm. Intraoperative graft viability was primarily assessed by monitoring cold ischemia time, reperfusion response, time to spontaneous cardiac contraction, contraction strength, hemodynamic stability, and the presence of anastomotic leakage.

Criteria for successful cardiac reperfusion included: (i) recovery of spontaneous heartbeat after reperfusion, with low-energy defibrillation if necessary for rhythm stabilization; (ii) strong cardiac contractions with a reddish, well-perfused appearance; and (iii) maintenance of stable intraoperative blood pressure and hemodynamics.

Renal Transplantation

The recipient's left kidney fascia was dissected to expose the renal artery and vein, which were isolated and clamped. After division, the renal vessels were cut and flushed with heparinized saline. The upper ureter was ligated, and the left kidney was excised. The donor kidney, wrapped in ice-cold gauze with its vessels exteriorized, was placed in the left renal fossa. The donor renal artery and vein were trimmed and anastomosed end-to-end with the recipient's left renal vessels using 8-0 polypropylene sutures. Reperfusion was then initiated, and graft visibility was confirmed observing adequate vascular filling.

The donor ureter was attached to a silicone catheter, which was exteriorized through a flank stoma and fixed in place. After confirming the absence of bleeding or leak-

Table 1. Immunosuppressive and supportive medication regimen provided to the recipient.

Drug	Administration time	Dosage and route	Remarks
Methylprednisolone	POD 0–7 (postoperative day 0–7)	10 mg/kg (POD 0), 6 mg/kg QD (POD 1–3), 3 mg/kg QD (POD 4–7), intravenous injection (i.v.)	Rapid perioperative immunosuppression and inflammation control
Rituximab	Preoperative	19 mg/kg, single intravenous infusion, with premedication for allergy prevention	B-cell depletion to reduce antibody-mediated rejection
Thymoglobulin (ATG)	POD 4–6	5 mg/kg per dose, diluted in 75 mL normal saline, intravenous infusion, for 3 days	T-cell suppression, rescue immunosuppressive intervention
Tacrolimus	Starting POD 1	0.25 mg every 12 hours, oral	Long-term T-cell mediated immunosuppression
Mycophenolate mofetil (MMF)	Starting POD 1	250 mg every 12 hours, oral	Inhibits lymphocyte proliferation, maintenance therapy
Low-molecular-weight heparin	Immediately postoperatively	500 IU every 12 hours, subcutaneous injection	Thrombosis prevention, adjusted per coagulation status
Cefoperazone-Sulbactam	Immediately postoperatively	0.25 g, intramuscular injection, twice daily	Bacterial infection prophylaxis; 7 days, followed by oral cephalosporin maintenance
Ganciclovir	Immediately postoperatively	5 mg/kg + 75 mL normal saline, intravenous infusion, once daily	Viral infection prophylaxis; 7 days intravenous, followed by oral maintenance
Omeprazole	Immediately postoperatively	5 mg intravenous, once daily	Gastric mucosal protection during immunosuppression; 7 days intravenous, followed by oral maintenance
Methoxyflurane	Immediately postoperatively	0.8 mg, intramuscular injection, every 12 hours	Analgesia: Continued for 7 days, then as needed (PRN)

age from both cardiac and renal anastomoses, an F22 rubber drain was placed in the right pelvic cavity. The abdominal wall was closed in layers and secured with pressure dressing. For the kidney, intraoperative assessment included cold ischemia time, reperfusion response, graft color and swelling, vascular patency, anastomotic integrity, and ureteral drainage. Successful renal reperfusion was defined as: (i) the graft appearing reddish and fully perfused upon restoration of blood flow; (ii) visible intraoperative urine output; and (iii) in cases without immediate urine production, subsequent postoperative urine output accompanied by a decrease in serum creatinine within several hours.

Immunosuppressive and Supportive Therapy for Recipients

The complete immunosuppressive and supportive regimen is summarized in Table 1. Preoperatively, B-cell depletion was achieved using a single intravenous dose of rituximab (19 mg/kg) after standard anti-allergy premedication. On the day of transplantation (postoperative day 0, POD 0), high-dose methylprednisolone (10 mg/kg, intravenous injection) was administered to enhance intraoperative and immediate postoperative immunosuppression. From POD 1 to POD 3, methylprednisolone was continued at 6 mg/kg/day i.v., and from POD 4 to POD 7, the dose was reduced to 3 mg/kg/day i.v. Starting on POD 1, oral tacrolimus (0.25 mg every 12 hours) and mycophenolate mofetil (MMF, 250 mg every 12 hours) were introduced as maintenance immunosuppressants. On POD 4, progressive ventricular wall thickening and renal enlargement were identified by ultrasound—strongly suggestive of acute rejection. Consequently, antithymocyte globulin (ATG; Thymoglobulin) was administered as rescue immunotherapy from POD 4 to POD 6. ATG was given at 5 mg/kg per dose, diluted in 75 mL of normal saline, and infused intravenously once daily for three consecutive days to rapidly suppress T cell activity.

To prevent postoperative thrombosis, subcutaneous low-molecular-weight heparin (500 IU Q12H) was initiated on the day of surgery. For antimicrobial prophylaxis, cefoperazone-sulbactam (0.25 g) was administered intramuscularly twice daily for 7 days, after which maintenance antibiotic therapy was transitioned to oral cephalosporins based on clinical progression.

For antiviral prophylaxis, ganciclovir (5 mg/kg) was diluted in 75 mL of normal saline and infused intravenously once daily for 7 days, followed by oral antiviral maintenance therapy. Supportive therapy included omeprazole (5 mg, i.v., once daily) for gastric mucosal protection, which was transitioned to oral administration after POD 7. Postoperative analgesia was provided with intramuscular meloxicam (0.8 mg every 12 hours) during the first 7 days and thereafter administered as needed (PRN).

Postoperative Monitoring and Experimental Endpoint Evaluation

Recipients were secured in a primate chair and lightly sedated as required to ensure stability. Vital signs—including heart rate, blood pressure, and oxygen saturation—were continuously monitored to comprehen-

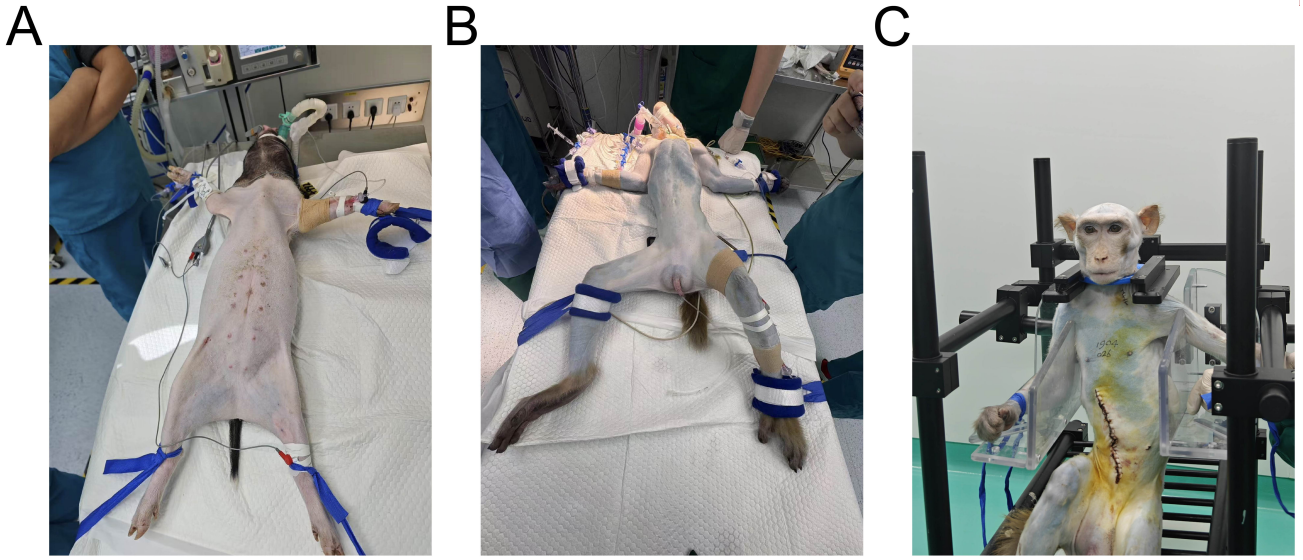

Fig. 1. Perioperative conditions of the donor and recipient. (A) Preoperative anesthesia and monitoring setup for the donor pig. (B) Preoperative anesthesia and monitoring setup for the recipient rhesus macaque. (C) Postoperative condition of the recipient macaque.

sively evaluate postoperative physiological status. Postoperative cardiac function was assessed using bedside transthoracic echocardiography (Vivid E95, GE Healthcare, Chicago, IL, USA), performed by the same cardiology-certified investigator to ensure data consistency. Echocardiographic assessment included measurement of ejection fraction (EF), left ventricular end-diastolic volume (LVEDV), and left ventricular wall thickness (LV wall thickness). Renal function was assessed with color Doppler ultrasonography (EPIQ 7C, Philips Healthcare, Andover, MA, USA) to determine the renal arterial resistive index (RI). Continuous multilead electrocardiographic monitoring was conducted using a bedside ECG system (IntelliVue MX800, Philips, Amsterdam, Netherlands).

The pleural and abdominal cavities were examined for fluid accumulation to verify proper graft perfusion and function. The experimental endpoint was defined as loss of renal graft blood flow and deterioration of donor heart function. At this stage, the animals were anesthetized and then euthanized with sodium pentobarbital (120 mg/kg, P3761, Sigma-Aldrich, St. Louis, MO, USA) administered through a central or peripheral vein, and delivered slowly until both respiration and cardiac activity ceased.

Blood samples were collected at predefined postoperative time points (0, 24, 48, 72, 120, 144, 168, and 171 hours) for hematological and coagulation analyses. Hematological parameters included white blood cell (WBC), red blood cell (RBC), and lymphocyte (Lym) counts. In contrast, coagulation was assessed by measuring prothrombin time (PT) and activated partial thromboplastin time (APTT). Blood specimens were obtained through peripheral or central venous puncture and anticoagulated with EDTA for hematological or sodium citrate for coagulation assays. Analyses were performed using an automated hematology analyzer (Sysmex XN-1000, Sysmex Corporation, Kobe, Hyogo, Japan) and a coagulation system (ACL TOP 700 CTS, Instrumentation Laboratory, Bedford, MA, USA), following the manufacturers' instructions.

Results

Perioperative Status and Postoperative Survival of the Recipient Monkey

We successfully performed a combined heart-kidney xenotransplantation from a porcine donor to a non-human primate recipient. The recipient was a healthy rhesus macaque (*Macaca mulatta*, ID: 11904026, body weight: 9.4 kg), and the donor was a genetically modified Bama miniature pig (*GTKO*/*SdaKO*/*CD46*/*CD55*/*TBM*, body weight: 7.9 kg). Preoperative preparations, including anesthesia induction and intraoperative monitoring for both donor and recipient, were conducted smoothly (Fig. 1A,B). The total procedure time was 257 minutes. Cardiac arrest lasted for 32 minutes, after which spontaneous cardiac rhythm was restored with a single 5 J defibrillation. Circulatory function remained stable throughout the procedure (Table 2).

The recipient's vital signs remained stable throughout surgery. However, mild bleeding was observed at the inferior vena cava anastomosis site, with an estimated blood loss of approximately 150 mL, which was effectively managed without causing circulatory instability. Intraoperative ACT levels remained above 200 seconds (baseline: 99 s; peak: 234 s), with no evidence of coagulopathy (Table 2).

Postoperatively, the tracheal tube was successfully removed 4 hours after recovery from anesthesia, and the monkey entered intensive postoperative monitoring. Vital signs remained within normal limits throughout the observation period. Under continuous supportive care and immunosuppressive therapy, the recipient survived for 7 days and

Table 2. Perioperative parameters and postoperative outcomes of the recipient monkey.

Parameter	Value	Time/Condition	Remarks
Recipient (monkey) body weight	9.4 kg	Preoperative	—
Donor (pig) body weight	7.9 kg	Preoperative	*GTKO/SdaKO/CD46/CD55/TBM* five-gene modified pig
Total surgery duration	257 min	Intraoperative	—
Cardiac arrest duration	32 min	Intraoperative	Recovered via single 5 J defibrillation
Blood loss	~150 mL	Intraoperative	Mild bleeding at inferior vena cava (IVC) anastomosis, promptly controlled
Activated clotting time (ACT)	200–234 s	Intraoperative	Baseline 99 s; maintained >200 s during surgery
Extubation	4 h post-op	Postoperative	After anesthesia recovery, stable vital signs
Survival	7 days 4 h	Postoperative	No severe adverse events observed

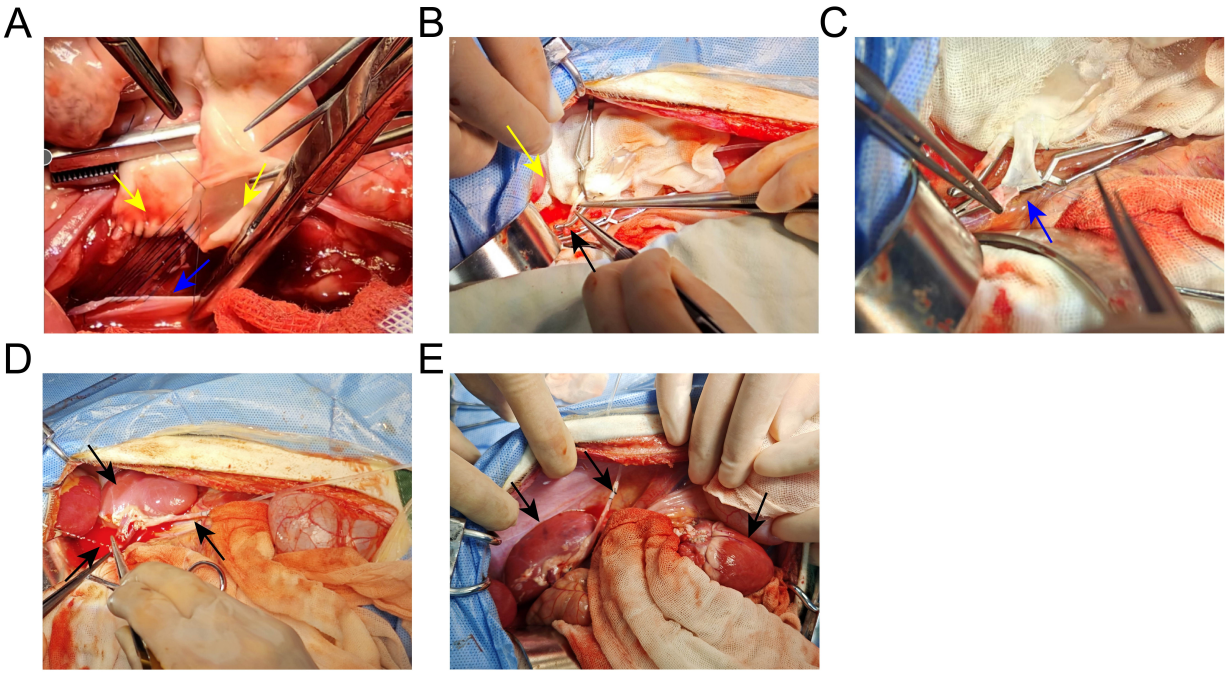

Fig. 2. Intraoperative views of the transplanted organs. (A) Cardiac transplantation. The anastomosis between the donor heart and the recipient's aorta has been achieved, while the donor pulmonary artery is being anastomosed to the recipient's inferior vena cava. Yellow arrows indicate arteries; blue arrow indicates veins. (B) Renal artery anastomosis. The renal artery (yellow arrow) is being continuously sutured, with a Bulldog clamp temporarily occluding the renal vasculature at the hilum (black arrow). (C) Renal vein (blue arrow) anastomosis. (D) Hemostasis following kidney transplantation. The upper arrow shows good perfusion and reddish coloration of the transplanted kidney. The lower left arrow points to a site of minor hemorrhage undergoing additional suturing. The lower right arrow indicates the ureter connected to a drainage stent. (E) Overview after completing cardiac and renal transplantation. The left arrow points to the kidney, the right arrow to the heart, and the middle arrow indicates the ureter exteriorized through the abdominal wall for urinary diversion.

4 hours after transplantation, without any serious adverse events (Fig. 1C, postoperative status of the recipient) (Table 2).

Intraoperative Graft Assessment

Vascular anastomoses and reperfusion of both the donor heart and kidney were successfully achieved. The cold ischemia times were 132 minutes for the donor heart and 210 minutes for the donor kidney.

During cardiac transplantation, the donor ascending aorta was anastomosed end-to-side to the recipient's abdominal aorta (Fig. 2A, left arrow). In contrast, the donor pulmonary artery was connected end-to-side to the recipient's inferior vena cava (Fig. 2A, right arrow). Upon release of the aortic clamp, the donor heart resumed spontaneous contractions, exhibiting strong pulsation and a healthy pink coloration, consistent with good perfusion.

For kidney transplantation, the renal artery was anastomosed with continuous suturing, and a Bulldog clamp was applied at the root of the recipient's left renal vessels to control bleeding (Fig. 2B). The renal vein was then anastomosed end-to-end, with the interface clearly visi-

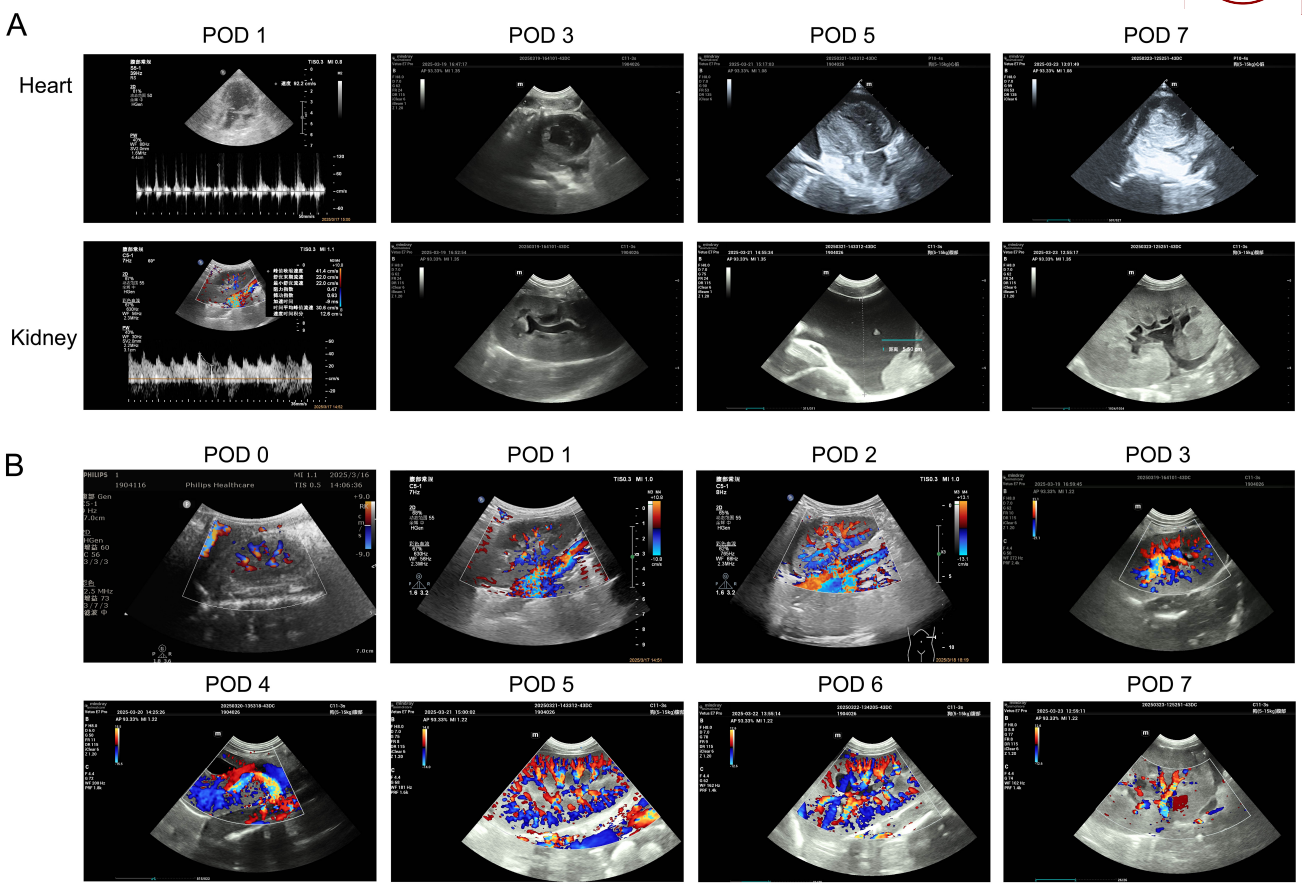

Fig. 3. Imaging and quantitative analysis of functional changes in combined heart–kidney xenografts post-transplantation. (A) Representative ultrasound images of the transplanted heart and kidney at different postoperative time points (POD 1, POD 3, POD 5, and POD 7). (B) Renal Doppler ultrasound showing blood flow changes from POD 0 to POD 7.

ble (Fig. 2C). Minor bleeding points were reinforced with additional sutures, and the donor kidney appeared well-perfused, full, and bright red. In contrast, the distal ureter was connected to a catheter to ensure unobstructed drainage (Fig. 2D).

By the completion of the procedure, both heart and kidney transplants were successfully positioned: the kidney placed on the left and the heart on the right, with the ureter exteriorized through the abdominal wall to form a stoma for postoperative drainage (Fig. 2E). No significant intraoperative complications, including hemorrhage or anastomotic leakage, were observed.

Early Postoperative Structural and Hemodynamic Assessment of Cardiac and Renal Grafts

To assess early functional changes following xenotransplantation, serial echocardiography and Doppler ultrasound were performed on the cardiac and renal grafts. On POD 1, the cardiac graft exhibited reduced EF, indicating early contractile dysfunction, while valvular structures, hemodynamics, and anastomotic patency remained intact. By POD 3, EF showed partial improvement, accompanied by reduced chamber size and thickening of the ventricular walls and interventricular septum. Blood flow velocity and direction were normal, with no evidence of thrombosis. On POD 5, EF stabilized at approximately 35%, with persistent thickening of the left ventricular free wall and interventricular septum, suggesting increased myocardial load, whereas chamber morphology and anastomotic flow remained unaltered. By POD 7, EF declined again, with progressive wall thickening and chamber reduction, although anastomotic flow remained unobstructed (Fig. 3A).

For the kidney graft, initial perfusion on POD 1 was reduced, with an elevated resistive index (RI); however, both normalized within hours, indicating a reversible hemodynamic compromise. By POD 3, the graft showed enlargement, cortical thickening, mild dilation of the ureter and renal pelvis, and perinephric fluid accumulation, findings consistent with urinary leakage. Despite these changes, perfusion remained stable with no hemodynamic deficits. On POD 5, the concentration of creatinine in the drained fluid increased to ~360 µmol/L (**Supplementary Material 1**), confirming urinary leakage while also demonstrating ongoing urine production by the graft. Parenchymal thickening persisted without deterioration in perfusion.

By POD 7, graft volume further increased, RI rose, and Doppler ultrasound showed reversed arterial flow with no venous outflow, indicating rapid functional decline

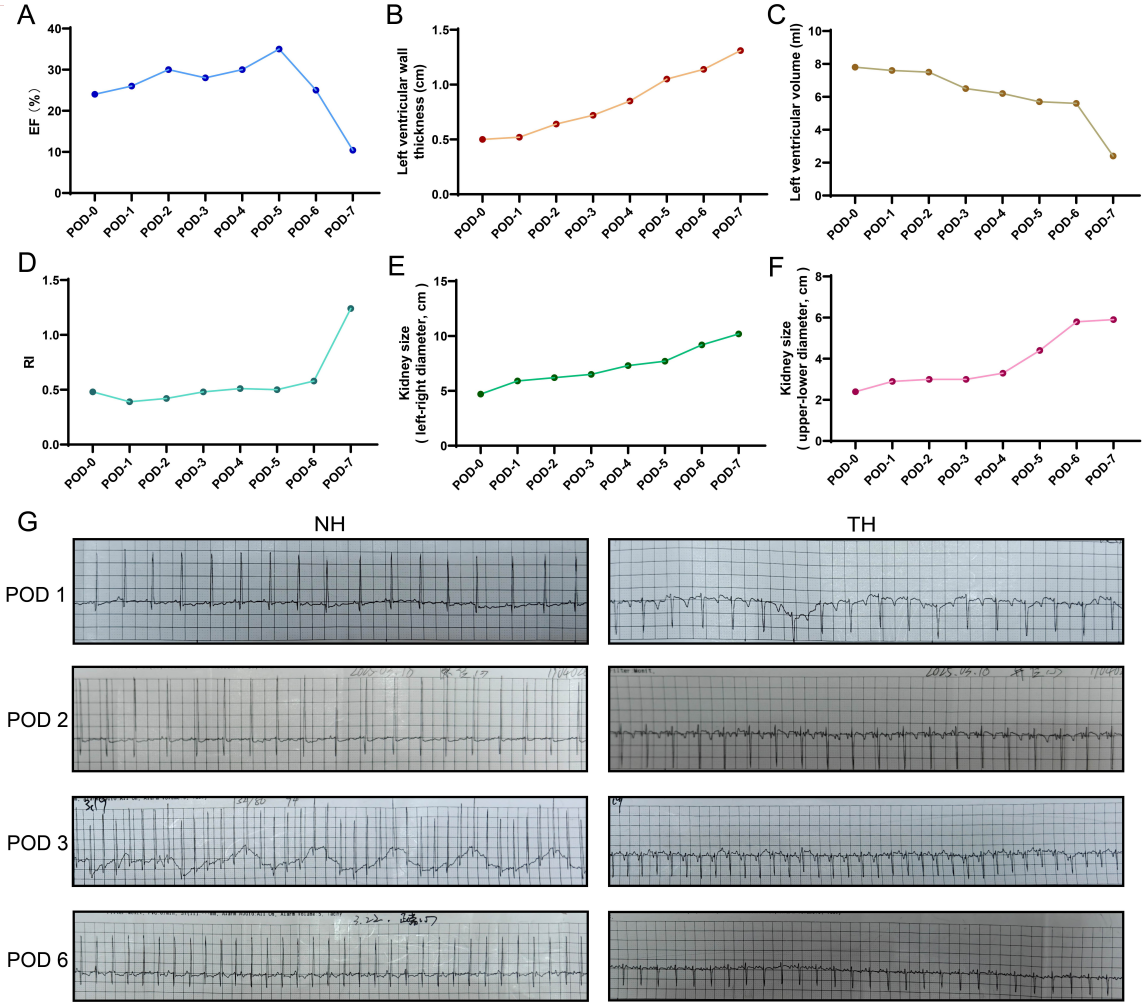

Fig. 4. Postoperative monitoring of cardiac and renal parameters in the recipient from POD 0 to POD 7. (A) Changes in ejection fraction (EF). (B) Left ventricular wall thickness. (C) Left ventricular volume. (D) Renal resistance index (RI). (E) Transverse renal graft dimension. (F) Longitudinal renal graft dimension. (G) Representative electrocardiographic (ECG) tracings. NH, native heart (recipient's own heart); TH, transplanted heart.

(Fig. 3A). Changes in renal blood flow are illustrated in Fig. 3B. From the day of surgery (POD 0) to POD 5, renal perfusion progressively improved and remained stable during early recovery. However, on POD 6, perfusion quality began to decline, leading to a significant reduction by POD 7.

Quantitative Dynamics of Postoperative Cardiac and Renal Function

During the early postoperative period, the cardiac graft exhibited dynamic changes in EF. On POD 1, EF was reduced, indicating early contractile impairment; from POD 2 to POD 5, EF gradually recovered, reaching its peak on POD 5, before declining again on POD 6–POD 7 (Fig. 4A). Concurrently, left ventricular (LV) wall thickness increased from 0.50 cm immediately after surgery to 1.31 cm by POD 7 (Fig. 4B), while LV volume decreased from 7.8 mL to 2.4 mL (Fig. 4C), reflecting progressive chamber contraction and myocardial hypertrophy.

Renal graft perfusion, assessed by the resistive index (RI), improved on POD 1, with the RI decreasing to 0.39. Between POD 2 and POD 5, RI remained relatively stable (0.42–0.51). On POD 6 and POD 7, RI increased to 0.58 and 1.24, respectively, with reversed diastolic flow, suggesting graft dysfunction or early rejection (Fig. 4D). The renal graft volume steadily increased, with the transverse diameter expanding from 4.69 cm to 10.20 cm and the longitudinal diameter from 2.41 cm to 5.90 cm. From POD 5 and POD 7, substantial enlargement was accompanied by perinephric fluid accumulation and mild pelvicalyceal dilation, consistent with urinary leakage and progressive graft dysfunction (Fig. 4E,F).

Continuous ECG monitoring during the early postoperative period demonstrated independent rhythmic activity of both the native heart (NH) and transplanted heart (TH), with no evidence of fusion (Fig. 4G). On POD 1, NH and TH rates were 130 and 128 bpm, respectively, both maintaining a regular rhythm. By POD 2, NH remained at 129

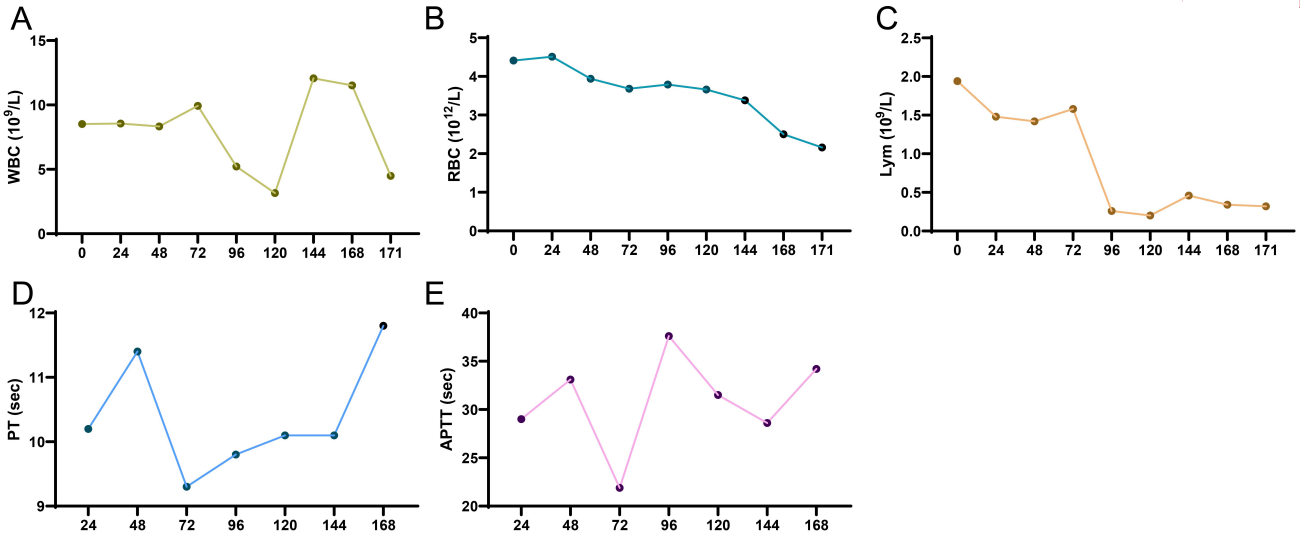

Fig. 5. Postoperative trends in hematologic and coagulation parameters. (A) White blood cell (WBC) counts from 0 to 171 hours post-transplantation. (B) Red blood cell (RBC) count from 0 to 171 hours post-transplantation. (C) Lymphocyte (Lym) counts from 0 to 171 hours post-transplantation. (D) Prothrombin time (PT) values from 24 to 168 hours postoperatively. (E) Activated partial thromboplastin time (APTT) values from 24 to 168 hours postoperatively.

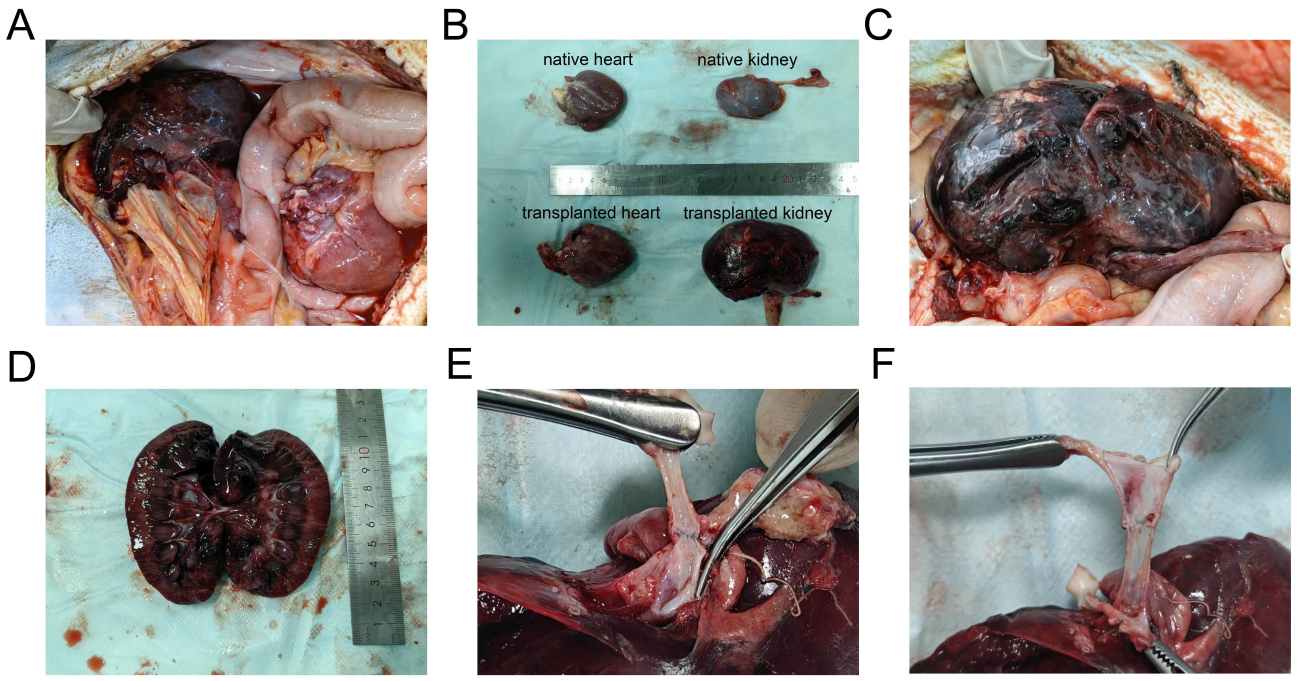

Fig. 6. Postoperative organ status and renal anatomy. (A) *In situ* view of the transplanted organs. (B) Comparison of native and transplanted heart and kidney. (C) External view of the transplanted kidney. (D) Anatomical dissection of the transplanted kidney showing preserved corticomedullary structure. (E) Renal artery anastomosis site. (F) Renal vein anastomosis site.

bpm, while TH increased to 135 bpm, indicating enhanced intrinsic pacemaker activity of the graft. On POD 3, both heart rates accelerated markedly (NH, 222 bpm; TH, 205 bpm). By POD 6, TH heart rate decreased to 163 bpm. Early postoperative QRS amplitudes in TH were relatively low (POD 1–POD 2), reflecting incomplete recovery of myocardial electrical activity. From POD 3 to POD 6, TH QRS amplitudes progressively increased, indicating gradual restoration of myocardial repolarization and contractile function; however, they remained lower than NH, likely due to graft myocardial edema, interstitial fluid accumulation, and ventricular wall thickening.

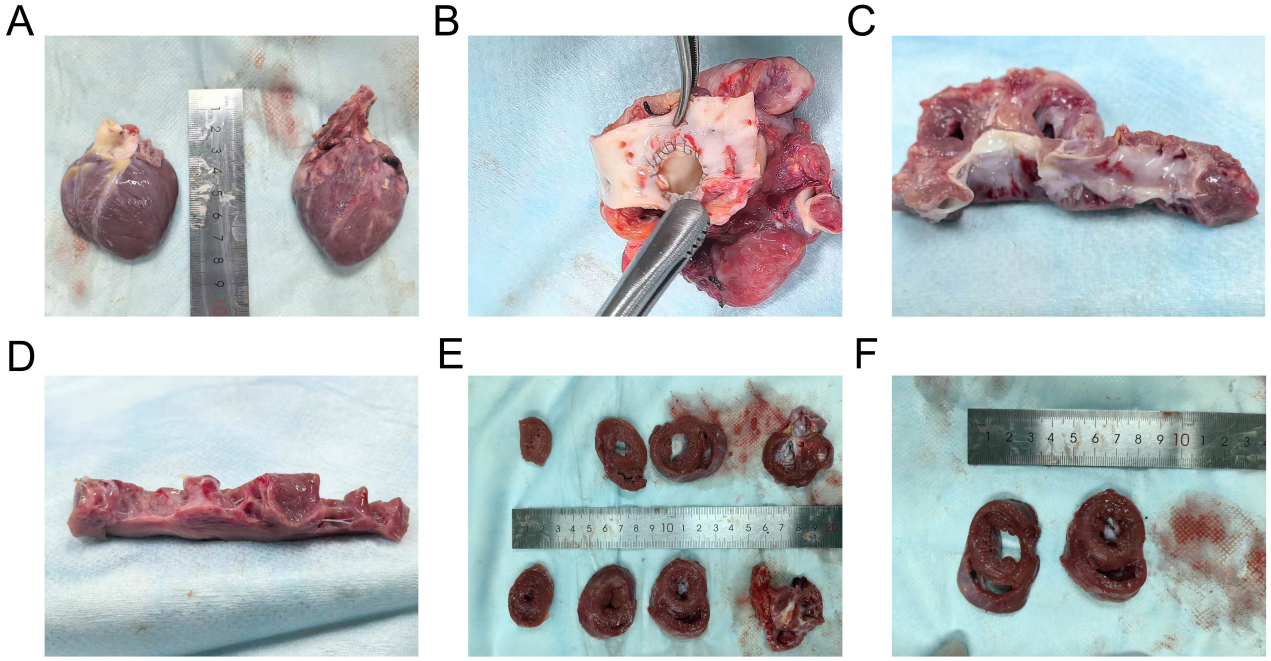

Fig. 7. Postoperative morphological and histological features of the transplanted heart. (A) Morphological comparison between native and transplanted hearts, showing significant enlargement of the graft. (B) Anastomosis between the donor ascending aorta and the recipient abdominal aorta; the site remains patent and thrombus-free. (C) Aortic and mitral valve structure of the transplanted heart; valves remain structurally intact with no signs of thickening, degeneration, or thrombosis. (D) Histological image showing myocardial hypertrophy in the transplanted heart. (E,F) Transverse section comparison between native and transplanted hearts; the graft exhibits notable ventricular wall edema and thickening.

Postoperative Hematologic and Coagulation Changes

Recipients exhibited dynamic fluctuations in hematological and coagulation parameters following combined heart–kidney xenotransplantation, reflecting shifts in immune and coagulation status postoperatively. The white blood cell (WBC) count remained relatively stable during the early postoperative period (0–48 hours), ranging between 8.3–8.5 $\times$ 10^9/L. A significant decline occurred by 72 hours, reaching a nadir of 3.16 $\times$ 10^9/L at 120 hours—likely due to bone marrow suppression from combined antimicrobial and immunosuppressive therapy. Subsequently, WBC levels surged, peaking at 12.07 $\times$ 10^9/L at 144 hours, suggesting a secondary infection or inflammatory rebound response. By 171 hours, WBC levels declined again, indicative of decompensated immune function and progression toward terminal status (Fig. 5A).

Red blood cell (RBC) count showed a continuous decline from 4.41 $\times$ 10^{12}/L preoperatively to 2.16 $\times$ 10^{12}/L at 171 hours postoperatively, indicating persistent hematopoietic impairment (Fig. 5B). Lymphocyte count (Lym) dropped sharply from 1.94 $\times$ 10^9/L preoperatively to 0.2 $\times$ 10^9/L at 120 hours, and remained critically low thereafter (0.32 $\times$ 10^9/L at 171 hours), reflecting adequate immunosuppression but also increased infection risk and rapid clinical deterioration in the later postoperative phase (Fig. 5C).

Under prophylactic anticoagulation with low-molecular-weight heparin, prothrombin time (PT) remained relatively stable (9.3–11.8 s), suggesting preserved function of the prothrombin-dependent coagulation pathway (Fig. 5D). Conversely, activated partial thromboplastin time (APTT) exhibited considerable variability, with significant prolongation observed between 72–96 hours and 144–168 hours (maximum 37.6 s), indicative of potential coagulopathy or consumptive coagulopathy (Fig. 5E).

Terminal Evaluation and Gross Morphology of Transplanted Grafts

According to the predefined experimental endpoint, the study was terminated upon complete cessation of blood flow to the donor kidney. On postoperative day 7, 4 hours, the recipient animal was euthanized under general anesthesia by open abdominal exsanguination, followed by systematic organ inspection. At terminal necropsy, both grafts were found in stable positions within the recipient's body. The donor heart exhibited robust contractions (**Supplementary Material 2**), whereas the kidney showed features of hemorrhagic infarction (Fig. 6A).

Comparison of the orthotopic (native) and transplanted organs revealed significant differences in size and morphology. The native heart and kidney weighed 35.40 g and 20.76 g, respectively, whereas the transplanted heart and kidney were significantly enlarged, weighing 49.00

g and 127.90 g, and exhibited well-demarcated, full, and turgid morphology (Fig. 6B). Sagittal sectioning of the transplanted kidney revealed clearly defined cortical and medullary structures (Fig. 6C,D). Examination of renal vascular anastomoses confirmed the integrity of both the arterial and venous junctions, with no evidence of hemorrhage or disruption (Fig. 6E,F).

Cardiac Graft Structural Analysis and Postoperative Adaptation

Further anatomical dissection of the transplanted heart revealed evidence of structural remodeling and postoperative adaptation. The transplanted heart was notably larger than the native heart, with apparent morphological differences (Fig. 7A). The donor ascending aorta was anastomosed to the recipient's abdominal aorta, and the anastomotic site remained intact, indicating unobstructed blood flow without thrombus formation (Fig. 7B). Both the aortic and mitral valves were well-preserved, with no evidence of leaflet thickening, degeneration, or mural thrombi (Fig. 7C). Furthermore, histological examination demonstrated a significant increase in myocardial thickness compared to the native heart (Fig. 7D). Cross-sectional analysis further revealed substantial myocardial edema and ventricular wall thickening, most prominent in the left ventricular free wall and interventricular septum (Fig. 7E,F).

Discussion

We successfully established a combined heart–kidney xenotransplantation model using five-gene-edited pigs (*GTKO*/*SdaKO*/*CD46*/*CD55*/*TBM*) as donors and rhesus macaques as recipients, achieving stable early graft function and a survival time of 7 days and 4 hours. In the early postoperative phase, the grafts demonstrated favorable physiological function, characterized by vigorous cardiac contractions and well-perfused kidneys producing urine, indicating that the model achieved its intended short-term objectives. However, over time, pathological changes developed in the recipient, including reduced renal perfusion and myocardial thickening. Imaging revealed a progressive increase in the renal resistance index, indicating compromised graft perfusion, potentially driven by immune rejection, endothelial injury, or increased local tension secondary to urinary retention. Notably, renal graft rejection occurred earlier than cardiac graft dysfunction. The transplanted heart retained partial function even after the onset of renal failure, remaining contractile at the time of necropsy. These findings suggest a potential immunoprotective advantage or adaptive response of the cardiac graft. This model not only provides a valuable platform for advancing fundamental xenotransplantation research and clinical translation but also highlights the differential kinetics of organ-specific rejection and the potential of multigene-editing strategies in prolonging xenograft survival.

This novel model addresses a critical gap in research on multi-organ xenotransplantation. While most prior studies have focused on single-organ xenografts, particularly the heart and kidney, which are the common targets for end-stage organ replacement therapy in clinical practice [14,15], the combined transplantation model presented here better reflects the clinical scenario of multiple organ failure. Notably, our model revealed an earlier onset of renal rejection (POD 7) relative to cardiac functional decline, suggesting fundamental differences in the immunologic susceptibility of these organs. This temporal disparity may be attributed to the heart's unique immune-privileged status, with cardiomyocytes expressing high levels of immunomodulatory molecules such as human leukocyte antigen-G (HLA-G), whereas the kidney, with its dense vascular endothelium, is more readily exposed to antibody-mediated injury [9,16,17]. Our findings are consistent with previously reported trends, although direct molecular evidence remains limited. Additionally, the heterotopic intra-abdominal cardiac transplantation technique employed in this study offers notable advantages. Unlike conventional intrathoracic transplantation, this approach reduces disruption of respiratory and circulatory function, thereby preserving the recipient's native cardiac output and providing a supportive window for graft recovery [18].

The five-gene-edited donor pigs used in this study (*GTKO*/*SdaKO*/*CD46*/*CD55*/*TBM*) represent a comprehensive gene modification strategy designed to overcome the primary immunological and coagulative barriers in xenotransplantation. *GTKO* (α1,3-galactosyltransferase knockout) and *SdaKO* (Sda synthase knockout) eliminate key xenoantigens responsible for hyperacute rejection [19,20]. The co-expression of human complement regulatory proteins CD46 and CD55 mitigates complement-mediated damage by inhibiting C3b/C4b deposition and accelerating the decay of C3/C5 convertases, respectively [21–23]. Additionally, the inclusion of human thrombomodulin (TBM) addresses the prothrombotic milieu and microvascular thrombosis (TMA) commonly observed in xenografts. TBM exerts anticoagulant and anti-inflammatory effects by activating the protein C pathway, thereby enhancing graft viability under procoagulant conditions [24].

Effective donor genetic engineering requires a multidimensional approach, encompassing antigen elimination, complement and coagulation regulation, modulation of inflammation and apoptosis, and overall immune regulation to ensure long-term xenograft survival. Recent evidence suggests that further removal of *CMAH* and *β4GALNT2*, combined with the expression of additional human immunomodulatory proteins (e.g., CD47, EPCR), in triple-knockout (*GGTA1*/*CMAH*/*β4GALNT2*) pigs significantly prolongs graft survival and reduces rejection and TMA in highly sensitized NHP models [25]. Future donor genome engineering should adopt an integrated strategy targeting antigen depletion, complement and coagulation balance, inflammation and apoptosis control, and immune modulation to advance the clinical translation of xenotransplantation.

A multi-modal immunosuppressive regimen was implemented, incorporating high-dose intraoperative and early postoperative methylprednisolone pulse therapy, followed by maintenance treatment using oral tacrolimus and mycophenolate mofetil (MMF), in conjunction with targeted lymphocyte-depletion strategies. This approach was designed to synergistically suppress T-cell, B-cell, and innate immune pathways, thereby maximizing inhibition of early xenogeneic immune responses. Despite this aggressive immunomodulation, characteristic signs of rejection appeared as early as POD 5, indicating persistent challenges in controlling the activation of the xenogeneic immune network.

From the perspective of cardiac function, the donor myocardium exhibited transient functional recovery during the initial reperfusion and early postoperative immunosuppression phase (POD 1–POD 3). However, progressive left ventricular wall thickening and a decline in ejection fraction by POD 7 suggest the onset of delayed graft rejection and myocardial remodeling. This pathological process may involve cytotoxic T-cell–mediated myocardial inflammation or antibody-mediated endothelial injury. Previous studies have reported delayed rejection in cardiac xenografts, often characterized by immune cell infiltration and xenograft vasculopathy [26,27], which aligns with our observations of reduced ventricular cavity size, increased wall thickness, and decreased EF. These alterations may also be partly attributable to ischemia–reperfusion injury (IRI), which has been linked to early functional impairment after cardiac xenotransplantation, highlighting the significant influence of perfusion protocols and cold ischemia time on graft recovery [28]. Both xenogeneic and allogeneic *ex vivo* perfusion models have revealed that markers of IRI—such as oxidative stress and reduced myocardial contractile pressure—correlate closely with functional deterioration [29].

In the kidney, increases in the resistance index (RI), reversed diastolic flow, and loss of renal venous return from POD 5 onward further underscore the limitations of the current immunosuppressive strategy in maintaining long-term xenograft function. Additionally, the persistent decline in peripheral lymphocyte counts (nadir at 0.2×10^9/L) indicates profound immunosuppression and possible steroid-induced bone marrow suppression, raising concerns for increased susceptibility to opportunistic infections. The subsequent rise in leukocyte count, along with clinical signs of infection, supports this concern. Moreover, significant fluctuations in APTT during POD 3–POD 4 and POD 6–POD 7 suggest potential depletion of coagulation factors or endothelial injury associated with immunosuppressive therapy. These findings underscore the critical need to balance the intensity of immunosuppression with hemostatic stability in the context of xenotransplantation.

Recent studies have shown that complement C5 inhibition with eculizumab significantly reduces the occurrence of TMA, a significant challenge in pig-to-human kidney xenotransplantation [30]. Our study did not include complement inhibition strategies, which may have contributed to the relatively early onset of rejection. Future strategies should incorporate advanced immunomodulatory approaches within the immunosuppressive regimen to achieve more comprehensive control of xenogeneic rejection across multiple immune pathways. Regarding T-cell modulation, while ATG provided early suppression, it did not selectively preserve regulatory T cells (Tregs). Tregs play a crucial role in establishing xenogeneic immune tolerance by secreting IL-10 and TGF-β to inhibit effector T-cell responses [31,32]. Strategies combining anti-CD154 monoclonal antibodies can promote stable expansion of Tregs, representing a key direction for inducing xenogeneic immune tolerance [33]. Future approaches could combine Treg monitoring with the inhibition of the CD40/CD154 axis to optimize the balance between immunosuppressive intensity and immune tolerance. Moreover, JAK-STAT pathway inhibitors, such as tofacitinib and ruxolitinib, have shown efficacy in regulating inflammatory responses and T-cell activation. When integrated with donor-specific B-cell depletion strategies, these agents may further extend xenograft survival [34–36]. Future studies should focus on new strategies targeting T and B cells, the complement system, and innate immunity, coupled with functional immune monitoring, including Treg ratios, DSA changes, and coagulation parameters, to enable personalized, dynamically regulated, and precision-guided immunointervention.

In this study, the cardiac graft exhibited early postoperative systolic dysfunction, as indicated by a reduced EF, suggesting that intraoperative ischemia-reperfusion injury substantially affected myocardial performance. By POD 3, a partial recovery in EF was observed, implying a certain degree of reversibility in early ischemic injury and the capacity of the myocardium to initiate short-term repair mechanisms. During this period, ventricular chamber dimensions were reduced and wall thickness increased, potentially reflecting an early stress response and compensatory remodeling. On POD 5, EF reached its peak; however, cardiac function subsequently fluctuated and declined, with a notable decrease in EF by POD 7, accompanied by progressive ventricular wall thickening and further chamber constriction. These findings suggest that ongoing myocardial remodeling may contribute to impaired diastolic compliance and reduced pump efficiency, likely associated with myocardial edema, interstitial fluid accumulation, and concentric hypertrophy.

Gross pathological examination of the grafted heart revealed a tense appearance with markedly thickened myocardium, corroborating echocardiographic evidence of structural remodeling. The observed decline in EF, along with elevated QRS amplitude that did not return to baseline levels of the native heart, further indicates limited recovery of cardiomyocyte function—potentially due to postoperative interstitial edema, focal necrosis, or inflammatory cell infiltration [37]. Notably, no thrombus formation or anasto-

motic occlusion was observed during the early phase, indicating preserved graft perfusion and underscoring the efficacy of the *GTKO*/*SdaKO*/*CD46*/*CD55*/*TBM* genetic modifications in mitigating coagulopathic responses. Consistent with previous findings, the low expression of MHC class I molecules in cardiomyocytes and delayed infiltration of antigen-presenting cells (APCs) may offer an early "immune buffer window" for the cardiac graft [38–40].

Hemodynamic changes in the renal graft were precisely evaluated using Doppler ultrasound-derived RI. On POD 1, RI rapidly returned to the normal range, indicating reversibility of the initial perfusion disturbances. However, between POD 6 and POD 7, RI increased markedly to 1.24, accompanied by reversed diastolic flow, suggesting the onset of functional graft failure, likely due to acute rejection or compromised renal venous outflow. In parallel, renal arterial perfusion improved gradually until POD 5. However, it declined sharply from POD 6 onward, culminating in complete cessation of flow by POD 7, thereby delineating a clear imaging window for the end-point event.

Terminal pathology confirmed widespread hemorrhagic infarction of the renal parenchyma, with intact anastomotic structures, indicating that graft failure had primarily resulted from immune-mediated endothelial injury and microcirculatory collapse. Ultrasound findings, including substantial graft enlargement, pelvicalyceal system dilation, and perinephric fluid accumulation—together with rising serum creatinine—provided indirect evidence of residual renal function amid structural compromise. These ultrasonographic manifestations were consistent with the significantly increased post-transplant kidney weight (127.9 g) and pathological findings of hemorrhagic infarction, highlighting the high sensitivity and specificity of ultrasound for continuous postoperative graft monitoring.

A key finding of this study is the distinct kinetic patterns of rejection observed between cardiac and renal xenografts. While the renal graft exhibited complete loss of perfusion by POD 7, the cardiac graft retained partial function even after renal failure, highlighting organ-specific differences in susceptibility to xenogeneic immune responses. These differences may arise from multiple factors, including organ-specific antigen expression profiles, vascular architecture, patterns of immune cell infiltration, and intrinsic immunomodulatory mechanisms within each organ [41,42]. Consistent with our findings, previous studies on pig-to-human renal xenotransplantation have reported that renal grafts are particularly prone to TMA, a hallmark feature of xenograft rejection [30,43].

In contrast, the heart may possess superior adaptive capacity or intrinsic protective mechanisms that confer more resistance to immune-mediated injury [21]. Additionally, marked eosinophilic infiltration was observed in the pulmonary tissues of the primate recipients, suggesting that mucosa-associated lymphoid tissues may serve as immunological "frontline" sites for xenogeneic attack [44]. In this study, the renal graft was anatomically adjacent to intestinal lymphoid tissues, which may have accelerated antibody-mediated rejection.

Using a combined heart–kidney xenotransplantation model, this study establishes a crucial technical and evaluative foundation for functional assessment in orthotopic cardiac xenotransplantation. Donor hearts maintained autonomous contraction in a physiological circulation for over a week, while echocardiography enabled dynamic monitoring of EF fluctuations, perfusion, and structural remodeling, thereby providing a multidimensional framework for functional evaluation. The findings indicate that fluctuations in cardiac recovery are impacted not only by immune-mediated injury but also by ischemia–reperfusion effects, volume load, metabolic status, and immunosuppressive toxicity. These observations underscore the significance of sequential, integrated, multi-parameter monitoring rather than relying on single time points or static measures. Notably, cardiac and renal responses displayed significant heterogeneity. The heart demonstrated greater stability and resilience in maintaining hemodynamics and structural adaptation, whereas the kidney was more vulnerable to combined injury from immune responses and pressure overload. For future studies of orthotopic cardiac xenotransplantation, early evaluation should prioritize EF variability, chamber dimensions, and valvular integrity, supplemented by myocardial biomarker surveillance. This strategy may enable the development of precise early-warning models and optimization of individualized immunomodulation.

Despite providing novel insights into organ-specific features of xenograft rejection, this study has several limitations. First, although serial changes in blood cell counts and selected coagulation parameters were documented, critical indices such as platelet counts, D-dimer, and fibrinogen were not assessed. These markers are essential for detecting xenotransplantation-associated coagulopathies, including thrombotic microangiopathy, and their absence limits our ability to fully characterize dynamic alterations in the coagulation pathway during rejection. Second, the functional evaluation of the cardiac graft relied primarily on echocardiography, without complementary ECG tracings from either the recipient's native heart or the transplanted heart, which restricted comprehensive interpretation of the relationship between electrophysiological alterations and rejection responses.

Future optimization should focus on intraoperative cannula stabilization, standardized postoperative monitoring, and refinement of immunosuppressive protocols. Sustained sedation and precise drug administration are crucial for maintaining model stability, with central venous access for intravenous formulations combined with secure catheter fixation to prevent dislodgement. Postoperative care should incorporate high-frequency bedside ultrasound, along with complementary imaging approaches, such as blood gas analysis, radiography, CT scans, and MRI, to achieve comprehensive functional assessment. Laboratory monitoring should be streamlined to ensure continuous surveillance of

drug concentrations, electrolytes, and inflammatory mediators. From a mechanistic perspective, the observed divergence in cardiac and renal rejection warrants in-depth exploration. Approaches such as single-cell sequencing, cytokine profiling, and immune-subset tracking can delineate the cellular and molecular determinants, as well as the temporal dynamics, underlying these organ-specific responses.

Conclusion

We present a reproducible combined heart-kidney xenotransplantation model demonstrating short-term dual-graft viability, using five-gene-modified Bama miniature pigs as donors and rhesus macaques as recipients. Our findings demonstrate the technical feasibility and early functional maintenance of dual-organ xenotransplantation under immunosuppressive therapy. Both cardiac and renal grafts exhibited favorable perfusion and function in the early postoperative period. The results suggest that the heart may exhibit greater resistance to rejection in the context of combined transplantation; however, the underlying mechanisms, which may involve immune regulation or perfusion-related advantages, remain to be explored. Future studies should focus on delineating the temporal dynamics and regulatory pathways of multi-organ immune rejection and improve model stability, ultimately supporting the development of clinically viable strategies for long-term functional xenogeneic co-transplantation.

Availability of Data and Materials

The data that support the findings of this study are available from the corresponding authors upon reasonable request.

Author Contributions

LCY, ZD, XJW, and HC conceived and designed the study. LCY, ZD, CZ, JFW, LFY, JL contributed to data acquisition and surgical procedures. LHL, FLW, HFC contributed to clinical data analysis. GC contributed to animal experiments. LCY and ZD drafted the manuscript. XJW and HC critically revised the manuscript and supervised the overall study. All authors contributed to critical revision of the manuscript for important intellectual content. All authors read and approved the final manuscript. All authors have participated sufficiently in the work and agreed to be accountable for all aspects of the work.

Ethics Approval and Consent to Participate

All animal experiments were conducted at Haifeng Biotechnology Co., Ltd. (Chengdu, China), under facility license SYXK (Chuan) 2023-0271, and were approved by the Institutional Animal Care and Use Committee (approval number: IAC-202503[O-01]).

Acknowledgment

Not applicable.

Funding

This research received no external funding.

Conflict of Interest

The authors declare no conflict of interest.

Supplementary Material

Supplementary material associated with this article can be found, in the online version, at https://doi.org/10.24976/Discov.Med.202537202.211.

References

[1] Patel MS, Louras N, Vagefi PA. Liver xenotransplantation. Current Opinion in Organ Transplantation. 2017; 22: 535–540. https://doi.org/10.1097/MOT.0000000000000459.

[2] Stephan A. Organ Shortage: Can We Decrease the Demand? Experimental and Clinical Transplantation. 2017; 15: 6–9. https://doi.org/10.6002/ect.mesot2016.L27.

[3] Peterson L, Yacoub MH, Ayares D, Yamada K, Eisenson D, Griffith BP, *et al*. Physiological basis for xenotransplantation from genetically modified pigs to humans. Physiological Reviews. 2024; 104: 1409–1459. https://doi.org/10.1152/physrev.00041.2023.

[4] Yuan Y, Cui Y, Zhao D, Yuan Y, Zhao Y, Li D, *et al*. Complement networks in gene-edited pig xenotransplantation: enhancing transplant success and addressing organ shortage. Journal of Translational Medicine. 2024; 22: 324. https://doi.org/10.1186/s12967-024-05136-4.

[5] Iwanczyk Z, Vasudev K, Cozzi E, Cooper DKC. Contributions of Europeans to Xenotransplantation Research: 1. Pig Organ Xenotransplantation. Transplant International. 2025; 38: 14041. https://doi.org/10.3389/ti.2025.14041.

[6] Ali A, Kemter E, Wolf E. Advances in Organ and Tissue Xenotransplantation. Annual Review of Animal Biosciences. 2024; 12: 369–390. https://doi.org/10.1146/annurev-animal-021122-102606.

[7] Mohiuddin MM, Corcoran PC, Singh AK, Azimzadeh A, Hoyt RF, Jr, Thomas ML, *et al*. B-cell depletion extends the survival of GTKO.hCD46Tg pig heart xenografts in baboons for up to 8 months. American Journal of Transplantation. 2012; 12: 763–771. https://doi.org/10.1111/j.1600-6143.2011.03846.x.

[8] Cooper DKC, Mou L, Bottino R. A brief review of the current status of pig islet xenotransplantation. Frontiers in Immunology. 2024; 15: 1366530. https://doi.org/10.3389/fimmu.2024.1366530.

[9] Singh AK, Goerlich CE, Zhang T, Lewis B, Hershfeld A, Braileanu G, *et al*. Genetically engineered pig heart transplantation in non-human primates. Communications Medicine. 2025; 5: 6. https://doi.org/10.1038/s43856-025-00731-y.

[10] Adams AB, Kim SC, Martens GR, Ladowski JM, Estrada JL, Reyes LM, *et al*. Xenoantigen Deletion and Chemical Immunosuppression Can Prolong Renal Xenograft Survival. Annals of Surgery. 2018; 268: 564–573. https://doi.org/10.1097/SLA.0000000000002977.

[11] Mohiuddin MM, Goerlich CE, Singh AK, Zhang T, Tatarov I,

Lewis B, *et al*. Progressive genetic modifications of porcine cardiac xenografts extend survival to 9 months. Xenotransplantation. 2022; 29: e12744. https://doi.org/10.1111/xen.12744.

[12] Iwase H, Klein EC, Cooper DK. Physiologic Aspects of Pig Kidney Transplantation in Nonhuman Primates. Comparative Medicine. 2018; 68: 332–340. https://doi.org/10.30802/AALAS-CM-17-000117.

[13] Zhao W. Pig organs in humans: a forum on xenotransplantation. National Science Review. 2024; 11: nwae208. https://doi.org/10.1093/nsr/nwae208.

[14] Zhang X, Wang L, Zhang HT, Yang ZX, Yue SQ, Yang YL, *et al*. Preliminary report of preclinical trial of multi-genome engineering pig-to-macaque heart, liver and kidney transplantation. Organ Transplantation. 2021; 12: 51–56.

[15] Zhang G, Wang H, Guan YL, Yan J, Li J, Li XL, *et al*. 5 Gene editing pig-monkey xenotransplantation experiment report. Chinese Journal of Thoracic and Cardiovascular Surgery. 2024; 40: 379–384. (In Chinese)

[16] Yamamoto T, Hara H, Ayares D, Cooper DKC. The problem of the "4th xenoantigen" after pig organ transplantation in nonhuman primates may be overcome by expression of human "protective" proteins. Xenotransplantation. 2021; 28: e12658. https://doi.org/10.1111/xen.12658.

[17] von Bibra C, Hinkel R. Non-human primate studies for cardiomyocyte transplantation-ready for translation? Frontiers in Pharmacology. 2024; 15: 1408679. https://doi.org/10.3389/fphar.2024.1408679.

[18] Goerlich CE, DiChiacchio L, Zhang T, Singh AK, Lewis B, Tatarov I, *et al*. Heterotopic Porcine Cardiac Xenotransplantation in the Intra-Abdominal Position in a Non-Human Primate Model. Scientific Reports. 2020; 10: 10709. https://doi.org/10.1038/s41598-020-66430-x.

[19] Mohiuddin MM, Singh AK, Goerlich CE. Preclinical rationale and current pathways to support the first human clinical trials in cardiac xenotransplantation. Human Immunology. 2023; 84: 34–42. https://doi.org/10.1016/j.humimm.2022.07.001.

[20] Du j, Feng H, Chen G, Wang Y, Pan D. 216.1: Preparation of GTKO/SdaKO/CMAHKO/hCD46/hCD55/hTHBD pig with high expression level of human CD55 through a transgene strategy. Transplantation. 2023; 107: 50.

[21] Singireddy S, Tully A, Galindo J, Ayares D, Singh AK, Mohiuddin MM. Genetic Engineering of Donor Pig for the First Human Cardiac Xenotransplantation: Combatting Rejection, Coagulopathy, Inflammation, and Excessive Growth. Current Cardiology Reports. 2023; 25: 1649–1656. https://doi.org/10.1007/s11886-023-01978-4.

[22] Jagdale A, Nguyen H, Li J, Burnette K, Ayares D, Cooper DKC, *et al*. Does expression of a human complement-regulatory protein on xenograft cells protect them from systemic complement activation? International Journal of Surgery. 2020; 83: 184–188. https://doi.org/10.1016/j.ijsu.2020.09.034.

[23] Kim DD, Song WC. Membrane complement regulatory proteins. Clinical Immunology. 2006; 118: 127–136. https://doi.org/10.1016/j.clim.2005.10.014.

[24] Mohiuddin MM, Singh AK, Corcoran PC, Thomas Iii ML, Clark T, Lewis BG, *et al*. Chimeric 2C10R4 anti-CD40 antibody therapy is critical for long-term survival of GTKO.hCD46.hTBM pig-to-primate cardiac xenograft. Nature Communications. 2016; 7: 11138. https://doi.org/10.1038/ncomms11138.

[25] Manook M, Olaso D, Anwar I, DeLaura I, Yoon J, Bae Y, *et al*. Prolonged xenokidney graft survival in sensitized NHP recipients by expression of multiple human transgenes in a triple knockout pig. Science Translational Medicine. 2024; 16: eadk6152. https://doi.org/10.1126/scitranslmed.adk6152.

[26] Kuwaki K, Tseng YL, Dor FJMF, Shimizu A, Houser SL, Sanderson TM, *et al*. Heart transplantation in baboons using alpha1,3-galactosyltransferase gene-knockout pigs as donors: initial experience. Nature Medicine. 2005; 11: 29–31. https://doi.org/10.1038/nm1171.

[27] Kobayashi T, Taniguchi S, Neethling FA, Rose AG, Hancock WW, Ye Y, *et al*. Delayed xenograft rejection of pig-to-baboon cardiac transplants after cobra venom factor therapy. Transplantation. 1997; 64: 1255–1261. https://doi.org/10.1097/00007890-199711150-00005.

[28] Patel PM, Connolly MR, Coe TM, Calhoun A, Pollok F, Markmann JF, *et al*. Minimizing Ischemia Reperfusion Injury in Xenotransplantation. Frontiers in Immunology. 2021; 12: 681504. https://doi.org/10.3389/fimmu.2021.681504.

[29] Charniot JC, Bonnefont-Rousselot D, Albertini JP, Zerhouni K, Dever S, Richard I, *et al*. Oxidative stress implication in a new ex-vivo cardiac concordant xenotransplantation model. Free Radical Research. 2007; 41: 911–918. https://doi.org/10.1080/10715760701429775.

[30] Jones-Carr ME, Fatima H, Kumar V, Anderson DJ, Houp J, Perry JC, *et al*. C5 inhibition with eculizumab prevents thrombotic microangiopathy in a case series of pig-to-human kidney xenotransplantation. The Journal of Clinical Investigation. 2024; 134: e175996. https://doi.org/10.1172/JCI175996.

[31] Yang ZF, Ngai P, Lau CK, Ho DW, Tam KH, Lam CT, *et al*. Induction of long-term liver allograft survival by delayed immunosuppression is dependent on interleukin-10. Liver Transplantation. 2007; 13: 571–578. https://doi.org/10.1002/lt.21091.

[32] Levings MK, Bacchetta R, Schulz U, Roncarolo MG. The role of IL-10 and TGF-beta in the differentiation and effector function of T regulatory cells. International Archives of Allergy and Immunology. 2002; 129: 263–276. https://doi.org/10.1159/000067596.

[33] Ma D, Hirose T, Rosales I, Sasaki H, Colvin R, Markmann J, *et al*. Successful long-term TMA- and rejection-free survival of a kidney xenograft with triple xenoantigen knockout plus insertion of multiple human transgenes. Transplantation. 2020; 104: S82.

[34] Habibabady Z, McGrath G, Kinoshita K, Maenaka A, Ikechukwu I, Elias GF, *et al*. Antibody-mediated rejection in xenotransplantation: Can it be prevented or reversed? Xenotransplantation. 2023; 30: e12816. https://doi.org/10.1111/xen.12816.

[35] Kim JM, Kang SJ, Hong SH, Chung H, Shin JS, Min BH, *et al*. Long-term control of diabetes by tofacitinib-based immunosuppressive regimen after allo islet transplantation in diabetic rhesus monkeys that rejected previously transplanted porcine islets. Xenotransplantation. 2024; 31: e12850. https://doi.org/10.1111/xen.12850.

[36] Lee NK, Myeong SH, Hwang JW, Sa JK, Son HJ, Kim HJ, *et al*. Combination of Dexamethasone and Tofacitinib Reduces Xenogeneic MSC-Induced Immune Responses in a Mouse Model of Alzheimer's Disease. Biomedicines. 2022; 10: 1882. https://doi.org/10.3390/biomedicines10081882.

[37] Eisenson DL, Hisadome Y, Yamada K. Progress in Xenotransplantation: Immunologic Barriers, Advances in Gene Editing, and Successful Tolerance Induction Strategies in Pig-To-Primate Transplantation. Frontiers in Immunology. 2022; 13: 899657. https://doi.org/10.3389/fimmu.2022.899657.

[38] Lim B, Jang MJ, Oh SM, No JG, Lee J, Kim SE, *et al*. Comparative transcriptome analysis between long- and short-term survival after pig-to-monkey cardiac xenotransplantation reveals differential heart failure development. Animal Cells and Systems. 2023; 27: 234–248. https://doi.org/10.1080/19768354.2023.2265150.

[39] Lee SJ, Kim JS, Chee HK, Yun IJ, Park KS, Yang HS, *et al*. Seven Years of Experiences of Preclinical Experiments of Xeno-Heart Transplantation of Pig to Non-Human Primate (Cynomolgus Monkey). Transplantation Proceedings. 2018; 50: 1167–1171. https://doi.org/10.1016/j.transproceed.2018.01.041.

[40] Kamberi S, Meier RPH. Xenotransplantation literature update March 2023-November 2023. Xenotransplantation. 2024; 31:

e12837. https://doi.org/10.1111/xen.12837.

[41] Böhmig GA, Diebold M, Budde K. Opinions on the Future of Clinical Pig Kidney Xenotransplantation. Transplant International: Official Journal of the European Society for Organ Transplantation. 2024; 37: 13475. https://doi.org/10.3389/ti.2024.13475.

[42] Ganchiku Y, Riella LV. Pig-to-human kidney transplantation using brain-dead donors as recipients: One giant leap, or only one small step for transplantkind? Xenotransplantation. 2022; 29: e12748. https://doi.org/10.1111/xen.12748.

[43] Porrett PM, Orandi BJ, Kumar V, Houp J, Anderson D, Cozette Killian A, *et al*. First clinical-grade porcine kidney xenotransplant using a human decedent model. American Journal of Transplantation. 2022; 22: 1037–1053. https://doi.org/10.1111/ajt.16930.

[44] Litovsky SH, Foote JB, Jagdale A, Walcott G, Iwase H, Bikhet MH, *et al*. Cardiac and Pulmonary Histopathology in Baboons Following Genetically-Engineered Pig Orthotopic Heart Transplantation. Annals of Transplantation. 2022; 27: e935338. https://doi.org/10.12659/AOT.935338.